J Mater Sci (2011) 46:5184–5191
DOI 10.1007/s10853-011-5452-5

Non-isothermal crystallization of polyamide 6 matrix in all-polyamide composites: crystallization kinetic, melting behavior, and crystal morphology

Bozhen Wu · Ying Gong · Guisheng Yang

Received: 20 January 2011 / Accepted: 8 March 2011 / Published online: 15 March 2011

Abstract The difference in the melting points of polyamide 66 (PA66) fiber and polyamide 6 (PA6) film permits the preparation of all-polyamide (all-PA) composites by film-packing. Good interface performance and integrated consolidation structure in this all-PA composite are contributed to the similar chemical composition between PA66 fiber and PA6 matrix. In this paper, the non-isothermal crystallization kinetics and melting behaviors of PA6 matrix in all-PA composite are studied by differential scanning calorimetry (DSC), in which the modified Avrami equation, Ozawa model, and Mo equation combining Avrami and Ozawa equation are employed. It is found that the Mo equation exhibits great advantages in treating the non-isothermal crystallization kinetics for both neat PA6 and PA6 matrix in all-PA composite. The crystal morphologies of single PA66 fiber–PA6 composite by polarizing microscope (POM) clearly show a transcrystallinity layer of PA6 around PA66 fiber that proves a remarkable nucleation effect of PA66 fiber surface on the crystallization of PA6 matrix.

B. Wu · Y. Gong · G. Yang (✉)
Beijing National Laboratory for Molecular Sciences, Key Laboratory of Engineering Plastic, Joint Laboratory of Polymer Science and Technology, Institute of Chemistry, Chinese Academy of Sciences, Beijing 100080, China
e-mail: ygs20002000@yahoo.com

B. Wu · Y. Gong
Graduate School of the Chinese Academy of Sciences, Beijing 100080, China

G. Yang
Shanghai Genius Advanced Materials Co. Ltd, Shanghai 201109, China

Introduction

Recently, all-polymer composites, also named single polymer composites, that consist of polymer fibers reinforcing polymer matrix having same or similar composition [1] has gained much attention because it offers a possibility of better interface performance and recyclability than traditional glass or carbon fibers reinforced polymer composites [2]. Various polymers including polyolefin [3, 4], polyester [5, 6], and cellulose [7], etc., have been applied to prepare the all-polymer composites. Relying on the same or similar chemical composition and crystal structure between fiber and matrix in all-polymer composites, polymer fibers have a significantly effect on the crystallization of polymer matrix around the fibers and the phenomenon of transcrystallinity is also found in the all-polymer composites [8, 9]. However, no work about the crystallization kinetics of polymer matrix in the all-polymer composites has been done.

Polyamide (PA), as a well-known engineering plastic, has been used as the matrix of various fibers (such as glass [10, 11], carbon [12, 13], and aramid fibers [14, 15], etc.) reinforced composites to achieve higher performance. It is known that, when the composites undertake the applied load, the stress is transferred to the high-strength fibers through the fiber/matrix interface. Therefore, the mechanical properties of these fibers reinforced PA composites depend to some extent on the morphology and crystallinity of PA matrix in the fiber/matrix interface region [16]. Due to the semicrystalline nature of PA matrix and the heterogeneous-nucleation effect of fibers surface on PA matrix, the matrix around the fibers crystallizes normal to the fibers surface and the layer of transcrystallinity is formed in the interface of fibers reinforced PA composites [10, 17, 18].

In the case of all-polyamide (all-PA) composites, not enough work [19] has been done in comparison to the widespread application of PA materials. Therefore, in our lab, a film-stacking method based on the melting temperature difference of PA66 fiber and PA6 film has been developed to prepare all-PA composites [20]. Seeing that PA66 fiber has a melting temperature about 30 °C higher than that of PA6 film, the PA6 film can be fully melt to fill the gap between PA66 fibers and, however, the PA66 fibers remain the original high-orientation at a proper temperature that is higher than the melting temperature of PA6 film and lower than that of PA66 fiber. Because of the chemical similarity of the two components (sharing the same molecular structure unit: $–CONH–(CH_2)_5–$), good fiber/matrix interface bonding can be acquired and an obvious nucleation effect of fiber surface on the crystallization of matrix is observed in the resulting all-PA composites.

Based on the previous work, effect of PA66 fibers on the non-isothermal crystallization kinetics and the melting behaviors following crystallization of PA6 matrix in all-PA composites are studied by DSC in this paper. In addition, the morphology of PA6 matrix transcrystallinity around PA66 fibers by various cooling rates is investigated by POM.

Experimental

Materials and samples preparation

The properties of PA66 fibers and PA6 film and the detailed preparation methods for all-PA composites and single PA66 fiber–PA6 composites had been described in our previous work [20]. Briefly, a method of film-stacking was utilized to fabricate all-PA composites during which PA66 plain cloth and PA6 film were plied together in sequence and then PA6 film was melted at 235 °C to bond the PA66 fibers together. The PA66 fibers load in the all-PA composites was about 70 wt%.

Testing

The non-isothermal crystallization and melting process of the neat PA6 and the PA6 matrix in the resulting all-PA composites (hereinafter as PA6 matrix) were performed on a Perkin–Elmer Pyris Diamond DSC instrument as follows: the samples were heated from 25 to 235 °C at a rate of 50 °C/min and then kept for 5 min at this temperature to eliminate the heat history before cooling to 50 °C at a specified cooling rate of 1, 2, 5, 20, and 50 °C/min; after keeping at 50 °C for 5 min, samples were heated to 235 °C at a heating rate of 10 °C/min, followed by the next cooling and heating cycle. It is noteworthy that the temperature upper limit of 235 °C assured no melting PA66 fibers during the above process of heating the resulting all-PA composites. Three samples of PA66 fibers, PA6 film and the resulting all-PA composites was heated from 50 to 280 °C at a rate of 10 °C/min to obtain the melting curves, respectively. The non-isothermal crystallization of single fiber–polymer composite was implemented by the same procedure as on DSC. However, both the heating and cooling steps of single fiber–polymer composite were completed on a heating stage with N_2. The crystal microstructure of this composite was observed by POM (BX51, Olympus). Tensile fracture morphology of all-PA composites was observed by SEM (JEOL, Tokyo, Japan).

Results and discussion

Consolidation structure

In this paper, the all-PA composites sample for non-isothermal crystallization analysis was prepared at the molding temperature of 235 °C that was higher than the melting temperature of PA6 film and lower than that of PA66 fibers (see Fig. 1). Therefore, PA6 film was melt to fill in the voids between the unmolten PA66 fibers and bonded these fibers together by cooling during the preparing process. From Fig. 1, it is also observed that the

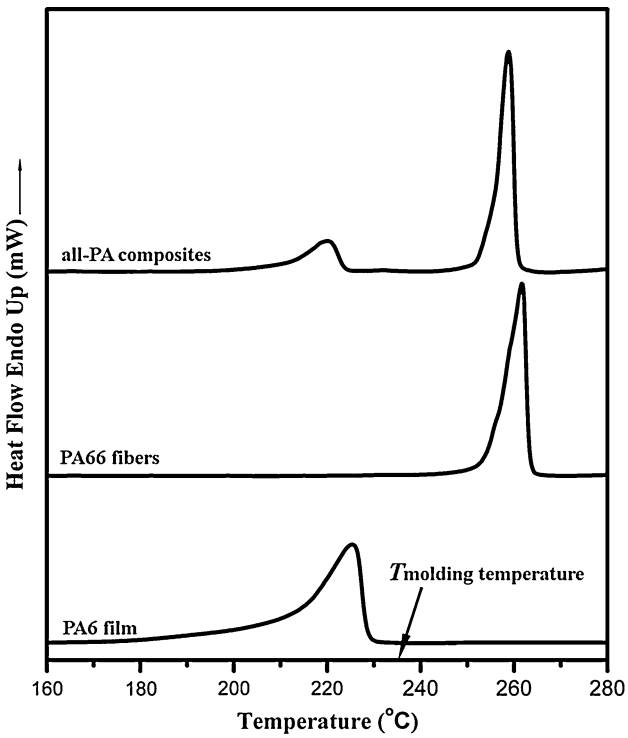

Fig. 1 Melting curves of all-PA composites, PA66 fibers and PA6 film

Fig. 2 Tensile fracture morphology of all-PA composites by SEM

resulting all-PA composites have two melting peaks which represent the melting of PA6 matrix and PA66 fibers, respectively. The complete consolidation structure of PA66 fibers reinforcing PA6 matrix in the resulting composites is further proved by the tensile fracture morphology as shown in Fig. 2: PA6 matrix adequately fills the voids inside the fiber bundle and between the fiber bundles; by cooling, PA66 fibers are effectively bonded together by PA6 matrix to form an integrated structure.

Non-isothermal crystallization kinetics

Due to the introducing of PA66 fibers in all-PA composites and the semicrystalline nature of PA6 matrix, it is presumable that PA6 matrix would present a different crystalline behavior from the neat PA6. In addition, it is considered that a non-isothermal cooling step is the closet to real industrial processing conditions. Therefore, in this study, the non-isothermal crystalline characteristic of PA6 matrix is investigated with comparison to neat PA6 by DSC.

The crystallization curves of neat PA6 and PA6 matrix at various cooling rates are shown in Fig. 3. It is not difficult to find that, in both cases, peak temperatures shift to lower temperature with cooling rate increasing. The detailed crystallization parameters (T_0 initial crystallization temperature, T_c crystallization peak temperature, D crystallization temperature range, and $t_{1/2}$ crystallization half time) are listed in Table 1. For both neat PA6 and PA6 matrix, increasing cooling rate results in the decrease of T_0, T_c, and $t_{1/2}$. It is more noteworthy that PA6 matrix possesses higher values of T_0, T_c, D, and $t_{1/2}$ than neat PA6 at the same cooling rate, which indicates to some extent that PA66 fibers in all-PA composites contribute to increasing the crystallization temperature and at the same time decreasing the crystallization rate of PA6 matrix. The higher crystallization temperatures are to be expected as a result of nucleation by a similar polymer, and the increased broadness in the crystallization exotherms may result from overlap of peaks from fiber-nucleated material and material nucleated in the melt.

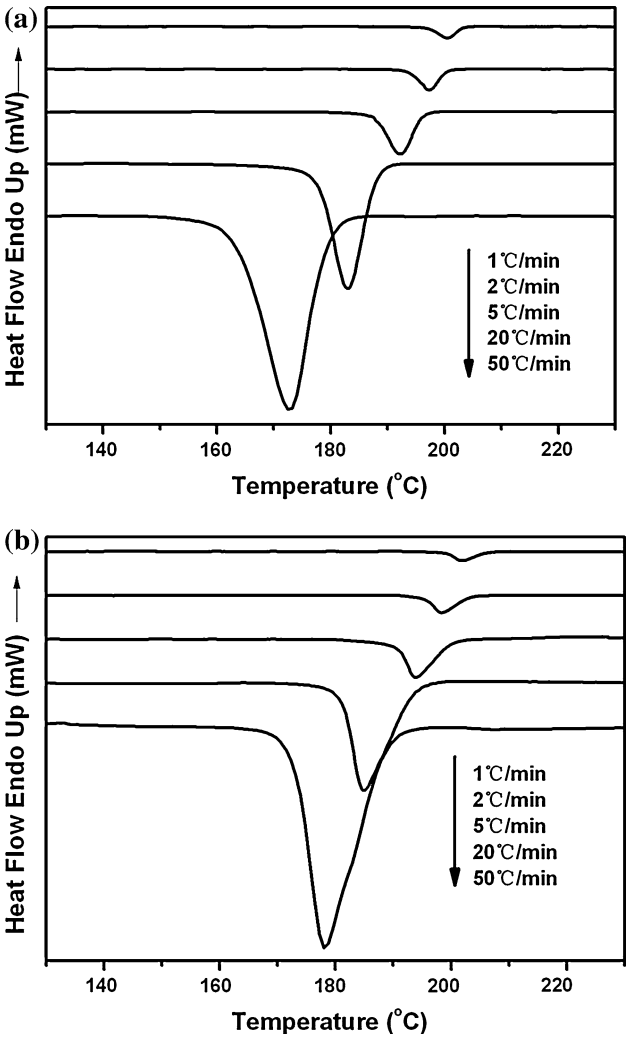

Fig. 3 Crystallization curves of **a** neat PA6 and **b** PA6 matrix at different cooling rates

Table 1 Values of T_0, T_c, D, and $t_{1/2}$ at various cooling rates for neat PA6 and PA6 matrix

Samples	Cooling rate (°C/min)	T_0 (°C)	T_c (°C)	D (°C)	$t_{1/2}$ (min)
Neat PA6	1	203.2	200.5	6.0	4.3
	2	200.4	197.3	4.0	3.0
	5	196.1	192.2	8.3	1.3
	20	188.0	182.9	10.3	0.4
	50	179.8	172.4	16.5	0.2
PA6 matrix	1	205.9	201.9	6.9	11.7
	2	203.1	198.4	7.6	10.8
	5	200.3	193.9	9.8	1.7
	20	193.7	184.8	12.7	0.6
	50	189.0	178.0	16.6	0.2

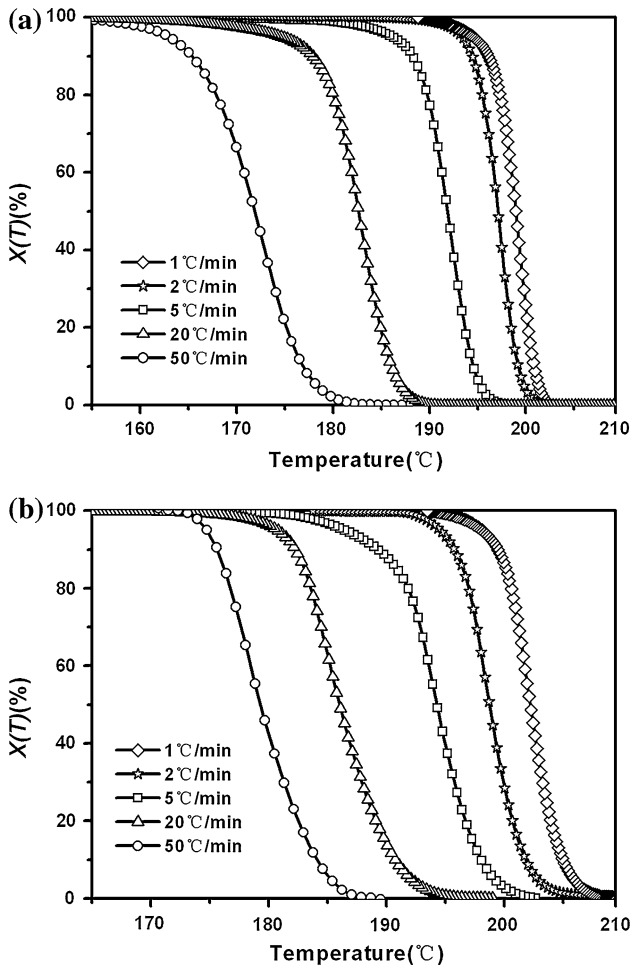

Fig. 4 Crystalline fraction of **a** neat PA6 and **b** PA6 matrix as a function of temperature

Based on the non-isothermal crystallization exothermal curves of neat PA6 and PA6 matrix, the integration of the exothermal peaks during the non-isothermal scan can give the relative crystallinity as a function of temperature as given in the equation below:

$$X(T) = \frac{H_T}{\Delta H_c} = \frac{\int_{T_0}^{T} (dH/dT)dT}{\int_{T_0}^{\infty} (dH/dT)dT} \times 100\% \quad (1)$$

where H_T and ΔH_c are the heat generated at the temperature of T and during the whole crystallization period, respectively, T_0 is the initial crystallization temperature and dH/dT is the heat flow rate. Figure 4 represents the crystalline fraction as a function of temperature for neat PA6 and PA6 matrix.

In addition, for the non-isothermal crystallization, the time t can be calculated from the temperature T as follows:

$$t = \frac{T_0 - T}{\varphi} \quad (2)$$

where T is the temperature at the time of t, and φ is the cooling rate. According to Eqs. 1 and 2, the time history of the relative crystallinity of neat PA6 and PA6 matrix at various cooling rates are shown in Fig. 5. All curves in Figs. 4 and 5 have the similar S or reversed S shape, which inflects the retardative effect of cooling rate on the crystallization [21].

In this paper, three models have been used to study the non-isothermal crystallization of PA6 that are the modified Avrami equation, Ozawa model, and Mo equation, respectively. Firstly, the modified Avrami equation such that

$$\log[-\ln(1 - X(t)/100)] = \log Z_t + n \log t \quad (3)$$

based on the assumption of constant crystallization temperature is used. In Eq. 3, Z_t is the rate constant during the non-isothermal crystallization process and n is the Avrami exponent. In Fig. 6, plots of $\log[-\ln(1 - X(t)/100)]$ versus $\log t$ for neat PA6 and PA6 matrix are shown, respectively. The obviously poor linearity for all plots reflects the

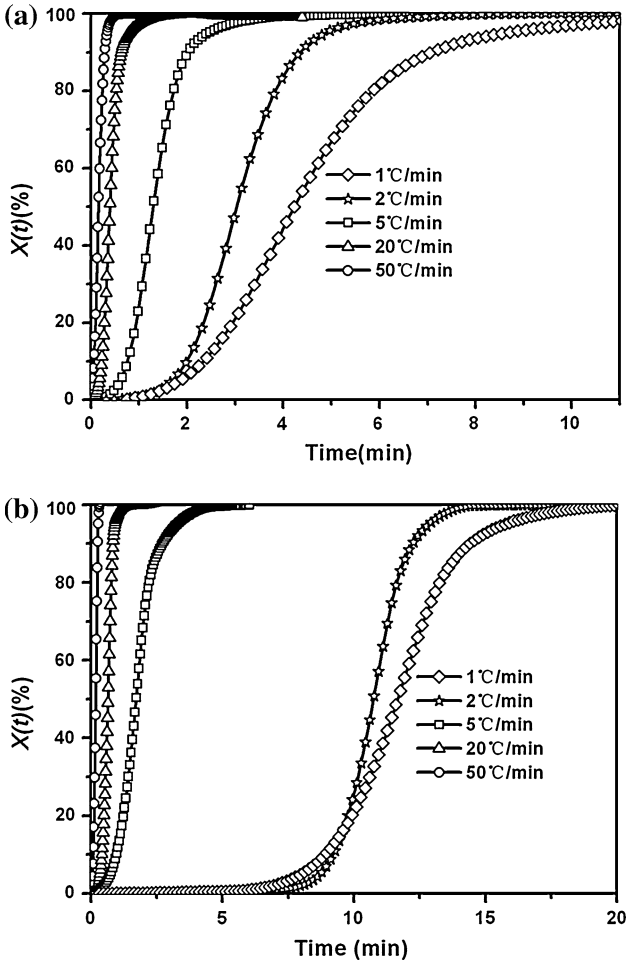

Fig. 5 Crystalline fraction of **a** neat PA6 and **b** PA6 matrix as a function of time

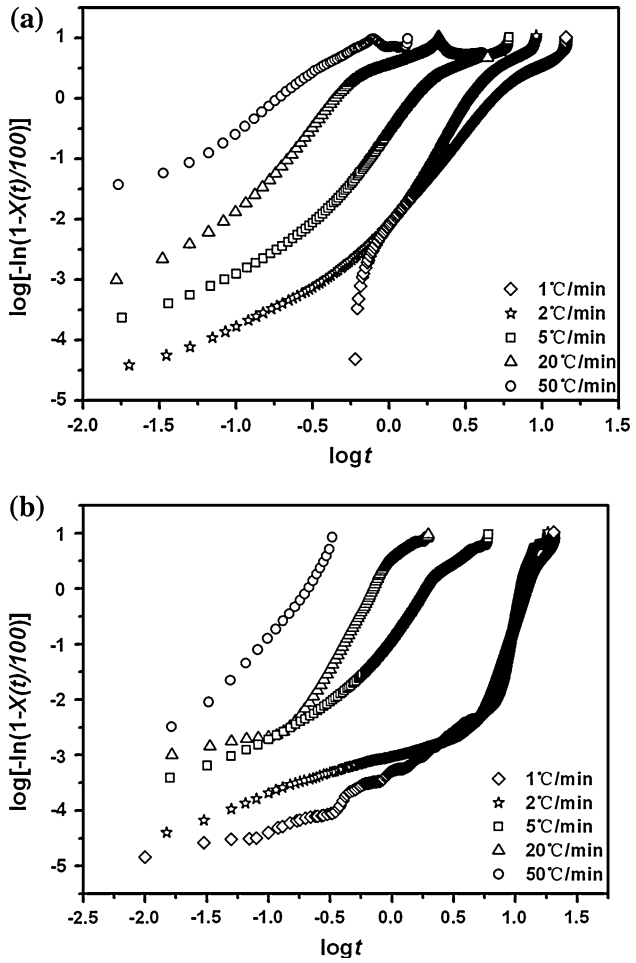

Fig. 6 Plots of $\log[-\ln(1 - X(t)/100)]$ versus $\log t$ for **a** neat PA6 and **b** PA6 matrix

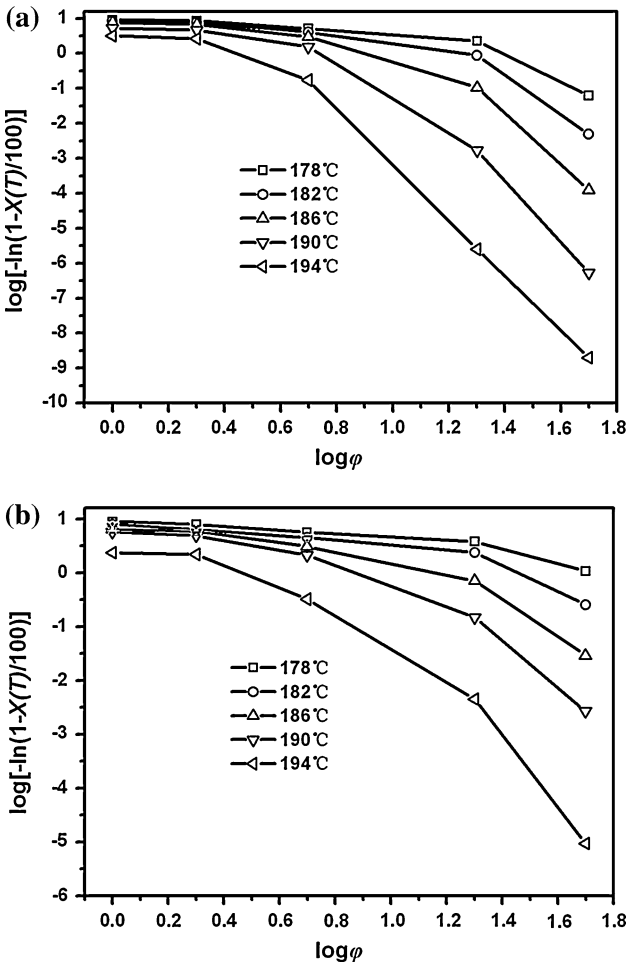

Fig. 7 Plots of $\log[-\ln(1 - X(t)/100)]$ versus $\log \varphi$ for **a** neat PA6 and **b** PA6 matrix

inadequacies of the modified Avrami equation to describe the non-isothermal crystallization for neat PA6 and PA6 matrix.

Secondly, Ozawa took the effect of cooling rate on the non-isothermal crystallization into consideration and developed the Avrami equation to describe the non-isothermal crystallization as follows [22]:

$$\log[-\ln(1 - X(T)/100)] = \log k(T) - m\log\varphi \tag{4}$$

where $k(T)$ is the cooling function related to the crystallization rate and m is the Ozawa exponent. Figure 7 illustrates the plots of $\log[-\ln(1 - X(T)/100)]$ as a function of $\log \varphi$. Obviously, all plots are not the straight lines. Therefore, it is concluded that the Ozawa model also fails to provide an adequate description of non-isothermal crystallization for both neat PA6 and PA6 matrix. The reason of this failure is that the crystallization rate during the non-isothermal crystallization is not constant.

From the above analysis, it is known that the modified Avrami equation and the Ozawa model are not suitable to investigate the non-isothermal crystallization of PA6, no matter neat PA6 or PA6 matrix. Therefore, Liu et al. [23] combined the Avrami and the Ozawa equations and put forward a new equation to describe the non-isothermal crystallization of polymers. This new equation can be simply expressed as follows:

$$\log \varphi = \log F(T) - a \log t \tag{5}$$

where $F(T) = [k(T)/Z_t]^{1/m}$, $a = n/m$. For the neat PA6 and PA6 matrix in this study, the plots of $\log \varphi$ versus $\log t$ are shown in Fig. 8. The good linearity of these plots verifies the success of this equation in describing the non-isothermal crystallization of PA6. The calculated values of $F(T)$ and a are listed in Table 2. It is worth mentioned that the value of $F(T)$ for neat PA6 is smaller than PA6 matrix when the crystalline fraction is same. The rate parameter $F(T)$ in Eq. 5 refers to the necessary value of cooling rate to achieve a determinate crystallinity at unit time for crystallization. Therefore, this difference in $F(T)$ of neat PA6 and PA6 matrix indicates that the crystallization rate of neat PA6 is faster than PA6 matrix.

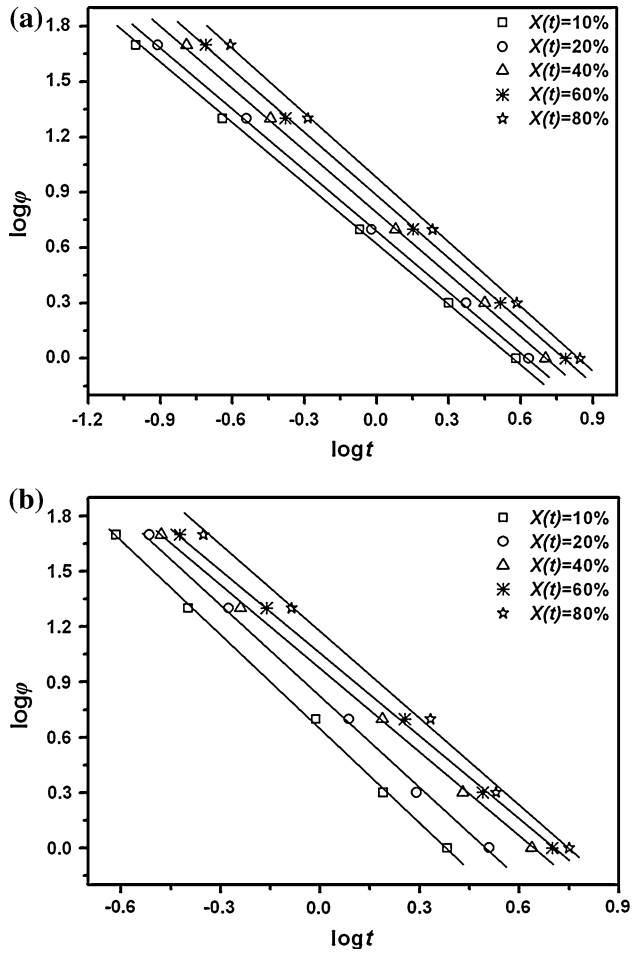

Fig. 8 Plots of log φ versus log t for **a** neat PA6 and **b** PA6 matrix at different crystallinity

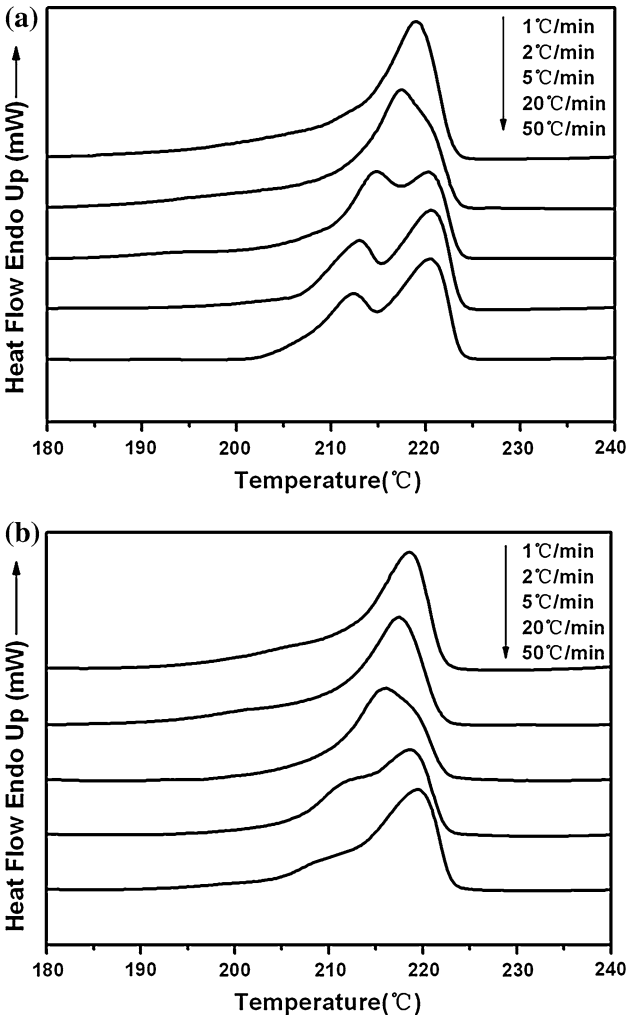

Fig. 9 Melting curves of **a** neat PA6 and **b** PA6 matrix following non-isothermal crystallization with various cooling rates by DSC

Table 2 Non-isothermal crystallization kinetics parameters by the Mo equation

$X(t)$ (%)	Neat PA6		PA6 matrix	
	a	$F(T)$	a	$F(T)$
10	1.0781	4.2170	1.7054	4.4978
20	1.1185	5.1050	1.6287	6.7453
40	1.1521	6.4551	1.5125	9.2257
60	1.1271	7.7090	1.5286	11.7490
80	1.3914	9.9770	1.5733	15.1356

Melting following non-isothermal crystallization

The heating curves of neat PA6 and PA6 matrix after non-isothermal crystallization with different cooling rates are shown in Fig. 9. It is found that both neat PA6 and PA6 matrix present double melting behaviors at the proper cooling rate. According to their positions, these two melting peaks are called high and low peak, respectively, for distinguishing. The detailed values of melting peak and melting enthalpy of neat PA6 and PA6 matrix are listed in Table 3.

It is well-known that PA6 has two common crystal forms melting about at 215 °C (γ-form) and 225 °C (α-form). The hydrogen bonding in the α polymorph is between antiparallel adjacent chains, and in the γ polymorph hydrogen bonding is between parallel chains [24]. Based on this melting temperature difference of α and γ crystal form, it is concluded that the high and low melting peaks here correspond to the melting of α and γ crystal form, respectively. The α phase that is thermodynamically the most stable is predominant in all samples, irrespectively the cooling rates. With increasing cooling rate, the γ crystal form appears and becomes more obvious. Comparing the melting peak and melting enthalpy of neat PA6 or PA6 matrix at various cooling rates, it is difficult to infer the effect of cooling rate on the degree of crystallinity, which is likely a result of a continuous thickening/perfection process in the T_g (glass transition temperature)–T_m for

the imperfect crystal formed at faster cooling [25]. However, position of the melting peak of γ crystal form shifts to lower temperature with raising the cooling rate for both neat PA6 and PA6 matrix that reflects to a certain extent the decrease of crystal thickness or perfection at faster cooling rate.

What is more noteworthy is that PA6 matrix always has lower T_m and ΔH_f than neat PA6 after the same cooling procedure. Based on this difference, it seems paradoxical that the presence of PA66 fibers, by causing an increase in the crystallization temperature, produces a small lowering of the melting temperature. However, such effects have been observed in other systems [26].

Table 3 Crystal parameters of neat PA6 and PA6 matrix after non-isothermal crystallization at various cooling rates

Samples	Cooling rate (°C/min)	T_m (°C)		ΔH_f (J/g)
		Low	High	
Neat PA6	1	–	219.1	50.8
	2	217.5	219.3	48.4
	5	214.5	220.3	49.3
	20	212.9	220.6	48.1
	50	212.1	220.5	50.9
PA6 matrix	1	–	218.7	47.9
	2	–	217.4	43.0
	5	214.7	217.9	43.0
	20	211.4	218.5	43.3
	50	209.2	219.5	45.8

Crystallographic morphology

From Table 1, it is found that PA6 matrix has slightly higher T_c than neat PA6 after the same cooling procedure. In order to explain the reason of this change of crystallization temperature, single PA66 fiber–PA6 composite was prepared on a glass slide and effect of cooling rate on the crystallographic morphology of this composite was investigated by POM equipped with a heating stage.

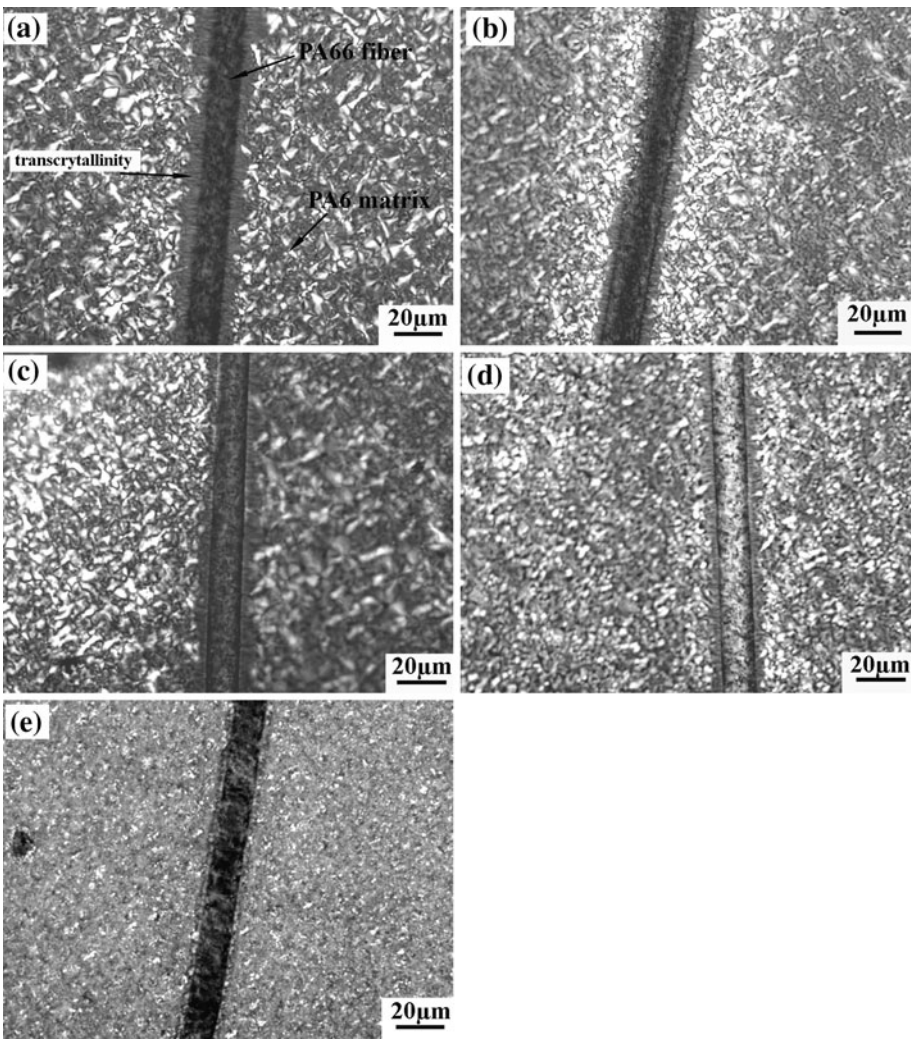

Fig. 10 Polarized microscopy of single PA66 fiber–PA6 composite after cooling at various rates: **a** 1 °C/min, **b** 2 °C/min, **c** 5 °C/min, **d** 20 °C/min, and **e** 50 °C/min

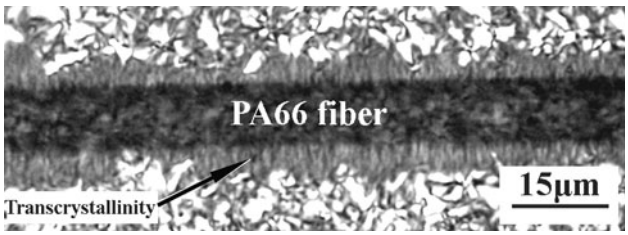

Fig. 11 Morphology of the transcrystallinity around PA66 fiber after cooling at 1 °C/min by a larger magnification

Figure 10 shows the crystalline morphologies of PA6 matrix in the resulting single PA66 fiber–PA6 composite after the given cooling step. When the cooling rate is lower than 50 °C/min, the obvious cross-extinction phenomenon is observed as shown in Fig. 10a–d. This cross-extinction phenomenon reflects the typical spherulitic crystal structure of PA6 after non-isothermal crystallization. In Fig. 10e, no cross-extinction is visible, which is because the faster cooling rate of 50 °C/min results in the smaller spherulites. Therefore, these smaller spherulites cannot be seen at the present magnification.

It is more important to mention that an especial morphology known as the transcrystallization different from the cross-extinction of PA6 matrix appears around the PA66 fiber for all samples. By a larger magnification, the morphology of the transcrystallinity is clearly seen in Fig. 11: many threadlike PA6 molecular chains are tightly arrayed around the PA66 fiber; all the chains are perpendicular to the PA66 surface. Due to the similar chemical nature and crystal structure between PA6 and PA66, sufficient nucleation center on the PA66 fiber surface can be offered for the crystallization of PA6 around the PA66 fiber. When cooling to below the initial crystallization temperature, PA6 molecular chains begin to array orderly to form the regular crystal structure. Nearby the PA66 fiber, the PA6 crystal preferentially grows around the nucleation centers on the fiber surface. As a result of the uniform and tight distribution of these nucleation centers, the orderly arrayed PA6 molecular chains can only grow along the radial direction of PA66 fiber. This existence of transcrystallinity layer also explains the higher crystallization temperature for PA6 matrix than neat PA6. Same as the influence of cooling rate on the size of PA6 spherocrystal, the thickness of PA6 transcrystallinity layer reduces with increasing the cooling rate.

Conclusions

By using three models to analyze the crystallization kinetic of PA6, it was concluded that the Mo equation combining Avrami and Ozawa equations could successfully describe the non-isothermal crystallization process of neat PA6 and PA6 matrix. The PA66 fibers surface offered sufficient nucleation centers for PA6 crystallization. Therefore, the crystallization temperature for PA6 matrix was higher than neat PA6 and a transcrystallinity layer was clearly observed around the PA66 fiber. In addition, the presence of tightly packing PA66 fibers in all-PA composites spatially hindered the orderly array of PA6 molecular chains that resulted in a slower crystallization of PA6 matrix than neat PA6. In brief, the nucleation mechanism, crystal growth, and final crystal form of PA6 matrix were changed by the presence of PA66 fibers in all-PA composites relative to neat PA6.

References

1. Capiati NJ, Porter RS (1975) J Mater Sci 10:1671. doi:10.1007/BF00554928
2. Pegoretti A, Zanolli A, Migliaresi C (2006) Compos Sci Technol 66:1970
3. ElMaaty MIA, Bassett DC, Olley RH, Hine PJ, Ward IM (1996) J Mater Sci 31:1157. doi:10.1007/BF00353094
4. Maity J, Jacob C, Das CK, Alam S, Singh RP (2008) Polym Test 27:581
5. Rasburn J, Hine PJ, Ward IM, Olley RH, Bassett DC, Kabeel MA (1995) J Mater Sci 30:615. doi:10.1007/BF00356319
6. Rojanapitayakorn P, Mather PT, Goldberg AJ, Weiss RA (2005) Polymer 46:761
7. Nishino T, Matsuda I, Hirao K (2004) Macromolecules 37:7683
8. Ishida H, Bussi P (1991) Macromolecules 24:3569
9. Loos J, Katzenberg F, Petermann J (1997) J Mater Sci 32:1551. doi:10.1023/A:1018578606510
10. Cartledge HCY, Baillie CA (1999) J Mater Sci 34:5099. doi:10.1023/A:1004713200894
11. Han KQ, Liu ZJ, Yu MH (2005) Macromol Mater Eng 290:688
12. Kurokawa M, Uchiyama Y, Iwai T, Nagai S (2003) Wear 254:468
13. Campbell M, Denault J, Yahia L, Bureau MN (2008) Compos Part A 39:796
14. Rath M, Kreuzberger S, Hinrichsen G (1998) Compos Part A 29A:933
15. Yu Z, Ait-Kadi A, Brisson J (1994) Polymer 35:1409
16. Bessell T, Shortall JB (1975) J Mater Sci 10:2035. doi:10.1007/BF00557481
17. Cartledge HCY, Baillie CA (1999) J Mater Sci 34:5113. doi:10.1023/A:1004765201803
18. Quan H, Li ZM, Yang MB, Huang R (2005) Compos Sci Technol 65:999
19. Hine PJ, Ward IM (2006) J Appl Polym Sci 101:991
20. Gong Y, Yang GS (2009) J Mater Sci 44:4639. doi:10.1007/s10853-009-3708-0
21. Liu XH, Wu Q (2002) Eur Polym J 38:1383
22. Ozawa T (1971) Polymer 12:150
23. Liu JP, Mo ZS, Qi YC, Zhang HF, Chen DL (1993) Acta Polym Sin 1:1
24. Weeding TL, Veeman WS, Veeman WS, Angad Gaur H, Huysmans WGB (1988) Macromolecules 21:2028
25. Khanna YP (1992) Macromolecules 25:3296
26. Bassett DC, Patel D (1994) Polymer 35:1855